# Investigating the Emergence of Dynamical Instabilities in the Bogoliubov-De-Gennes Equation; A Case Study of Different Boundary Conditions

Matriculation Number: 200003837[1]

PH:5103

[1]This research was conducted based on a model previously investigated by my supervisor Sang-Shin Baak. All code used to produce my results in this report was written by me but some code was verified against initial calculations performed by SangShin Baak.

# Contents

## Abstract

This thesis studies the emergence of dynamical instabilities in the Bogoliubov-De-Gennes equation. Using finite-difference methods (FDM) we explore numerically the linearised Bogoliubov-De-Gennes equation in a steady-state BEC analogue black hole model. We examine how this system changes under different boundary conditions by relating this set-up to those of black hole lasers, we show that these phenomena are in fact the same effect and explore the conditions under which this wave amplification occurs. Additionally, we find that under certain boundary conditions additional instabilities occur.


## Introduction

The unification of quantum theory and gravity is one of the greatest unsolved challenges in physics. Resolving their inconsistencies would provide a deeper understanding of the fundamental nature of spacetime. Progress requires examining physical scenarios where both theories play a significant role. Black holes warp spacetime more intensely than anywhere else in the universe, creating unique conditions for quantum and gravitational effects. The interplay between these effects leads to a range of phenomena, including Superradiance [1, 2, 3], Hawking radiation [4], and the Unruh effect [5], each of which provides insight into the quantum behaviour of curved spacetime. The event horizon of a black hole, a surface from which nothing inside can escape, is at the heart of many of these effects. Near the event horizon, Hawking radiation is emitted, causing black holes to gradually shrink and evaporate. Semiclassically, this radiation is thermal and carries no information about the black hole's interior. This conflicts with the fundamental principles of quantum mechanics. This problem is known as the Black Hole Information Paradox [6], and hints that a deeper understanding of black hole physics is needed.

Studying black holes directly presents significant challenges, effects such as Hawking radiation are extremely faint, overshadowed by the surrounding astrophysical environment, even by Cosmic Microwave Background Radiation [7]. This makes direct detection unlikely. To circumvent this, scientists have turned to analogue systems. Laboratory systems mimic spacetime curvature by creating an effective metric using the kinematic properties of certain media, allowing exploration of curved spacetime effects. In particular, these systems allow for access to measurements confined to the interior of a black hole, not possible for true black holes [8].

Analogue models were first proposed by Unruh in 1981 using water waves [9]. By creating a flowing region in water where the speed transitions from subsonic to supersonic (slower to faster than the speed of sound), a sonic horizon forms. This boundary obstructs sound waves from propagating against the current. Since then, analogue models have been explored in various physical systems, including superfluids, ultra-cold atoms, and optical setups [10] . However, analogue models are not perfect replicas of gravitational black

holes. Identifying the distinct properties of each system and the universal features shared with real black holes determines the extent to which they can provide meaningful insights. We will focus on Bose-Einstein Condensate (BEC) analogue models, see Sec.(1.1), which are inherently quantum mechanical and thus an ideal platform for studying quantum field effects in curved spacetime. BEC-based analogues have been extensively studied in the literature [11], and in 2016, the Steinhauer group experimentally observed a signature of Hawking radiation in a BEC-based system [12, 13].

Analogue models often exhibit instabilities in the form of complex-conjugate frequency modes, including quasinormal modes (QNMs) and dynamical instability modes (DIMs). QNMs are oscillations that decay exponentially over time, having a negative imaginary component to their frequency. These modes, while spatially unbounded, are stable and play a crucial role in the ringdown phase of black holes where energy is lost via radiation [14]. In contrast, their complex conjugate DIMs grow exponentially. These behaviours are often attributed to continued self-amplification discussed in Sec.(1.6). Often, these uncontrolled growths arise from the presence of negative energy modes. These modes can be excited within the medium, leading to the release of unbound energy. An example is the production of particle-antiparticle pairs, a phenomenon known as the Schiff-Snyder-Weinberg (SSW) effect. These effects have been extensively studied in black hole lasers [15, 16, 17, 18, 19]. This process is facilitated by the depletion of the background flow such that energy is still conserved. Analogue Hawking Radiation relies on small perturbations compared to the background for theoretical predictions to remain valid. If uncontrolled instabilities arise, the governing physics may deviate from the expected theoretical framework. If these instabilities disagree with experimental behaviours, it may indicate the need to look at more non-linear dynamics of the system. For example, the back reaction caused by these instabilities on the background spacetime curvature, these second-order effects are already being explored in the literature [20, 21, 22].

The main aims of this thesis are as follows: to combine and clarify dynamical instabilities, to showcase and discuss the instabilities of the Quasi-1D model, see Sec.(1.1) and to highlight the need for further investigation into dynamical instabilities. Previously, the 1D model was shown to induce instabilities [23], we characterise the nature of these instabilities by conducting a numerical investigation. Our findings indicate that these instabilities are associated with the presence of negative energy modes, see Sec.(2.2). In Sec.(8), we explain these modes in terms of Landau instability and conclude that this effect is qualitatively no different from that observed in black hole lasers. We compute directly the norm of eigenfrequencies and show the characteristic merging predicted by a two-mode approximation [24], see Sec.(1.3) for details. Finally, in Sec.(2.6), we discuss unexpected additional dynamical instabilities in Neumann and Robin boundary conditions. Ultimately, we extend the cases of black hole lasing, identify new instabilities, and illustrate clearly how dynamical instabilities occur.

# 1 BEC model

## 1.1 Derivation of Quasi-1D Finite model

Bose-Einstein condensates can be cooled to low temperatures such that all particles effectively occupy the ground state and can be described by a single wavefunction. The low-temperature nature of these means that we can model them effectively using the s-wave approximation. Particles are modelled by a contact interaction leading to an overall Hamiltonian, $H$ [25]:

$$H = \int d^3\boldsymbol{x}[\frac{\hbar^2}{2m}\nabla\Psi^\dagger\nabla\Psi + V_{ext}(\mathbf{x})\Psi^\dagger\Psi + \frac{g}{2}\Psi^\dagger\Psi^\dagger\Psi\Psi] \tag{1.1}$$

Where $g$ is the strength of the interactions modelled by a contact interaction, and $V_{\text{ext}}$ is an external potential. From this Hamiltonian, we can derive the familiar Gross-Pitaevskii equation(GPE), which governs the overall time-dependent dynamics of the system. Using the Heisenberg relation, $i\hbar\partial_t\Psi(t,x) = [\Psi(t,x), H]$, the GPE is given by:

$$i\hbar\frac{\partial\Psi(\mathbf{x},t)}{\partial t} = \left(-\frac{\hbar^2}{2m}\nabla^2 + V_{\text{ext}}(\mathbf{x}) + g|\Psi(\mathbf{x},t)|^2\right)\Psi(\mathbf{x},t). \tag{1.2}$$

We investigate the Quasi-1D Finite model in Figure (1). This one-dimensional model represents the simplest theoretical model of an analogue event horizon. A continuous source of condensate is present at $L_1$, and a drain is placed at $L_2$. This adds to the Hamiltonian a current term which results in a modified GPE equation featuring a source term, $J_e$:

$$i\hbar\frac{\partial\Psi(x,t)}{\partial t} = \left(-\frac{\hbar^2}{2m}\frac{\partial^2}{\partial x^2} + V_{\text{ext}}(x) + g|\Psi(x,t)|^2\right)\Psi(x,t) - J_e. \tag{1.3}$$

This GPE equation governs the condensate flow. The normalisation condition is given by $\int d^3x\,|\Psi(\mathbf{x},t)|^2 = N$ where N is the particle number. Propagating on the background are excited waves which can be derived by considering linear perturbations on the GPE, $\Psi(x,t) = \langle\Psi(x,t)\rangle + \tilde{\Psi}(x,t)$. The background condensate can be modelled in the Madelung representation as $\langle\Psi(x,t)\rangle = \sqrt{\rho}e^{-i\mu t+ivx}$ where $\mu$ is the chemical potential, $v$ is the fluid velocity and $\rho$ the fluid density [26]. It is important to note that the fluid velocity of this system is fixed along the entire flow, the Mach number of the substance is controlled by changing the speed of sound in the flow, $c = \sqrt{g\rho}$. We can freely factor the perturbation, we choose $\tilde{\Psi} = \sqrt{\rho}e^{-i\mu t+ivx}\psi$ where $\psi$ represent freely propagating waves. We choose the external potential to be $V_{\text{ext}} = \mu - g\rho - v^2/2$. Applying the Madelung representation to Eq.(1.3) and linearising in $\tilde{\Psi}$ , we can derive a form of

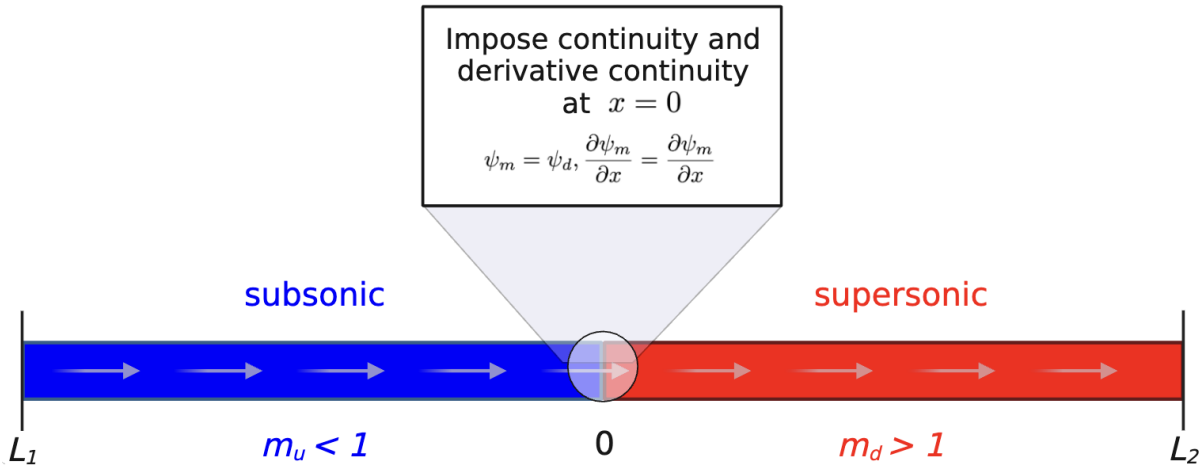


Figure 1: Quasi-1D model with a discontinuous flow. $m_{u(d)}$ represents the Mach number in the up(down)stream region. $L_1, L_2$ adjusts the length of the up and downstream regions. An analogue event horizon is defined when ($m_u$ or $m_d$) $> 1$. It is useful to consider regions in which the Mach number is greater than one as creating a cavity. This figure takes inspiration from [23]

the Bogoliubov-De-Gennes(BdG) equation, noting that the background satisfies Eq.(1.3) independently:

$$i\hbar\frac{\partial\psi}{\partial t} = (-\frac{\hbar^2}{2m}\frac{\partial^2}{\partial x^2} + iv\frac{\partial}{\partial x} + g\rho)\psi + g\rho\psi^* \tag{1.4}$$

The BdG can be rewritten using the Nambu spinor, $\Phi = (\psi, \psi^*)^t$ in a more compact form, where $\psi$ is related to the particles and $\psi^*$ the holes or anti-particles, these are Hermitian conjugates. To simplify the analysis, we set $\hbar = m = 1$:

$$i\sigma_3\frac{\partial\Phi}{\partial t} = (-\frac{1}{2}I\frac{\partial^2}{\partial x^2} - iv\sigma_3\frac{\partial}{\partial x} + g\rho\sigma_4)\Phi \tag{1.5}$$

We can rewrite this equation in terms of $m_u$, the upstream Mach number by dividing by the upstream speed of sound $c_u = \sqrt{g_u\rho} = 1$. (We work in units where this is taken as 1).

$$i\sigma_3\frac{\partial\Phi}{\partial t} = (-\frac{1}{2}I\frac{\partial^2}{\partial x^2} - im_u\sigma_3\frac{\partial}{\partial x} + \frac{g}{g_u}\sigma_4)\Phi \tag{1.6}$$

This equation describes the excited waves as seen from a stationary outside observer. We use the standard Pauli matrices for $\sigma_{1,2,3}$ and set $\sigma_4$ to the 2x2 matrix of ones. We can further rewrite this in a matrix form, looking for stationary solutions $\Phi = e^{-i\omega t}\Phi_\omega$:

$$i\frac{\partial\Phi}{\partial t} = \omega\Phi_\omega = H_{BdG}\Phi_\omega \tag{1.7}$$

.

## 1.2 Properties of Non-Hermitian BdG

The Bogoliubov-De-Gennes operator is $\sigma_3$-pseudo-Hermitian [27], meaning it satisfies a non-standard adjoint relation:

$$H_{BdG}^{\dagger} = \sigma_3 H_{BdG} \sigma_3^{-1} \tag{1.8}$$

The Pseudo-Hermitian symmetry of this system, unlike a Hermitian structure, does not restrict solutions to real frequencies. Instead, complex solutions can emerge in pairs. Using the fact that $\sigma_3 = \sigma_3^{-1} = \sigma_3^{\dagger}$ and considering a left eigenvector,$\tilde{\Phi}_\omega$, we can see this:

$$\sigma_3(\tilde{\Phi}_\omega H_{BdG})^{\dagger} = w^*(\sigma_3 \tilde{\Phi}_\omega^{\dagger}) = H_{BdG}(\sigma_3^{-1}\tilde{\Phi}_\omega^{\dagger}) \tag{1.9}$$

We can see that there exists a right vector for which $\omega^*$ is the eigenvalue, hence complex modes are allowed and will necessarily come in pairs [28]. The time evolution is also $\sigma_3$-pseudo-unitary, meaning it conserves with time an indefinite inner product or Krein product, which for real modes means it can be normalised to positive or negative, differing from a typical norm conserved in unitary systems.

$$\langle \Phi_n, \Phi_m \rangle = \int \Phi^{\dagger} \sigma_3 \Phi \; dx = \pm \delta_{n,m} \tag{1.10}$$

Using the Hermitian conjugate of Eq.(1.7), you can verify that this product is conserved, given it satisfies Eq.(1.8). Complex modes, however, have zero norm. Eq.(1.8) implies that $\langle \Phi_n, H_{BdG}\Phi_n \rangle = \langle \Phi_n H_{BdG}^{\dagger}, \Phi_n \rangle$ and therefore:

$$(\omega - \omega^*)\langle \Phi_n, \Phi_n \rangle^2 = 0 \tag{1.11}$$

The pseudo-Hermitian structure of the BdG equation allows for positive, negative and zero norms hence these equations can no longer be confined a Hilbert space instead we work in a Krein space [29].

## 1.3 Dynamical Instabilities & Mode Merging

Dynamical instabilities modes(DIMs) arise when linear perturbations, such as $\Phi$, grow exponentially in time or when eigenfrequencies acquire a positive imaginary component.

$$\omega = \omega_R + \omega_I i, \quad \omega_I > 0. \tag{1.12}$$

Dynamical instabilities can be related to the phenomenon of avoided crossing. For example, in energy eigenstates where levels approach each other but do not intersect due to a minimal distance enforced by their matching norm sign [30]. Conversely, when the

interacting modes have opposite norms, they are no longer repelled instead, their eigenvalues may coalesce and form a complex conjugate pair, a behaviour characteristic of the SSW instability mechanism. To study this phenomenon, we consider a two-mode approximation with unperturbed eigenmodes $\Phi_{\omega_1}$ and $\Phi_{\omega_2}$, coupled via an off-diagonal perturbation of magnitude $k$. The general state is written as a linear combination:

$$\Phi = a\Phi_{\omega_1} + b\Phi_{\omega_2} \tag{1.13}$$

This approximation is well-justified in the perturbative regime, as shown in [24] and has been applied previously in the Klein-Gordon Equation [31]. Since we are working with a restricted set of eigenfrequencies, we consider a restricted Hamiltonian:

$$\omega\Phi = H_{\mathrm{R,BdG}}\Phi = H_{\mathrm{R,BdG}}(a\Phi_1 + b\Phi_2) \tag{1.14}$$

Applying the restricted Hamiltonian operator yields the following matrix equation:

$$\omega\Phi = \begin{pmatrix} \omega_1 & k \\ k & \omega_2 \end{pmatrix} \Phi \tag{1.15}$$

$\omega_1$ and $\omega_2$ are the eigenstates of the unperturbed BdG Hamiltonian. $k$ is then the off-

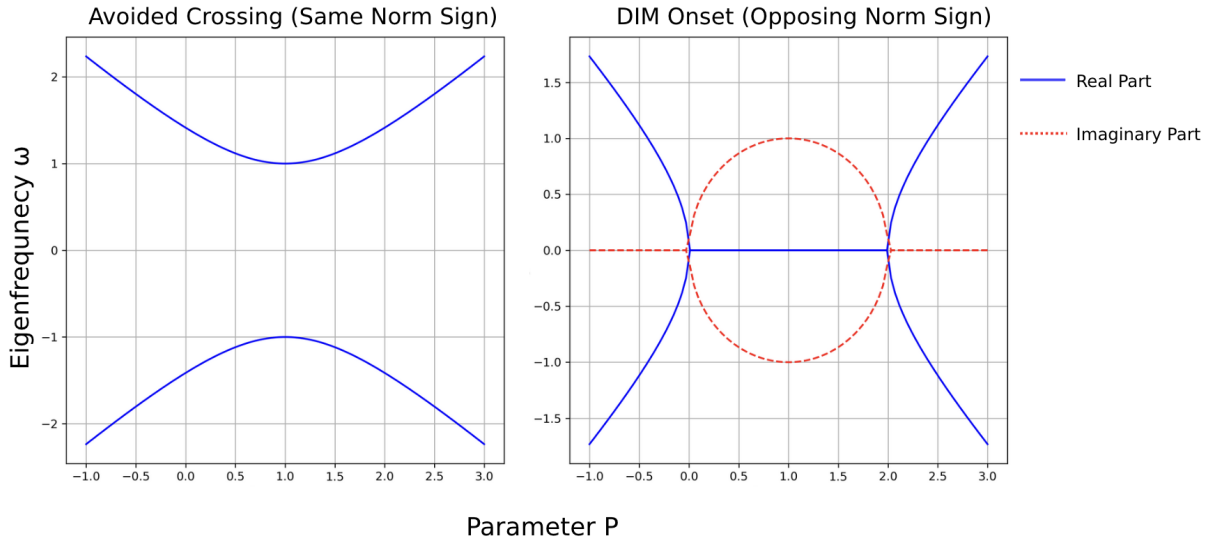


Figure 2: Avoided crossing and mode merging as the spacing between eigenfrequencies changes. P is an arbitrary parameter chosen to adjust the spacing between eigenvalues. $\omega_1 = 1 - P, \omega_2 = P - 1$. The coupling is given by $k^2 = \pm 1$, hence where on the left a minimum distance occurs on the right the instability is largest.

diagonal term, which is relevant when the spacing between eigenfrequencies $\omega_1 - \omega_2$ is small, the eigenvalue equation given by:

$$\omega = \frac{\omega_1 + \omega_2}{2} \pm \sqrt{(\omega_1 - \omega_2)^2 + k^2} \tag{1.16}$$

This expression reveals the conditions for dynamical instability. When the eigenvalues approach closely enough that $|k|^2 > (\omega_1 - \omega_2)^2$, the square root becomes imaginary, the resulting eigenfrequencies form a complex conjugate pair, $\omega = \omega_r \pm \omega_I i$ see Figure (2). This two-mode approximation describes well the emergence of DIMs within the BdG.

## 1.4 Fluid Dynamics

The BEC system can be expressed in terms of fluid dynamics using the Madelung representation in the GPE Eq.(1.2), our calculations take inspiration from [32]:

$$i\hbar\frac{\partial\Psi}{\partial t} = i\hbar(\frac{1}{2\rho}\frac{\partial\rho}{\partial t} - i\mu)\Psi = -\frac{\hbar^2}{2m}\frac{\partial^2\Psi}{\partial x^2} + V_{\text{ext}}\Psi + g\rho\Psi + J_e \tag{1.17}$$

Expanding $\frac{\partial^2\Psi}{\partial x^2}$ leads to two equations, by taking the imaginary part we arrive at a continuity equation:

$$\frac{\partial\rho}{\partial t} + \frac{\partial(\rho v)}{\partial x} = \text{Im}(\frac{\rho^2 J_e}{\Psi}) \tag{1.18}$$

The term on the left of Eq.(1.18) is a source/drain and vanishes except at the boundaries. We only consider stationary solutions, therefore, the condensate density will not vary with time, $\frac{\partial\rho}{\partial t} = 0$. By taking the real part, we can define a Quantum Euler's equation:

$$-\frac{\hbar}{2m\sqrt{\rho}}\frac{\partial^2\sqrt{\rho}}{\partial x^2} - \mu + \frac{\hbar v^2}{2m} + V_{\text{ext}} + g\rho = \text{Re}(\frac{J_e}{\hbar\Psi}) \tag{1.19}$$

This equation includes an additional Quantum pressure term $Q = -\frac{\hbar}{2m\sqrt{\rho}}\frac{\partial^2\sqrt{\rho}}{\partial x^2}$, this term describes how BECs resist compression due to their wavelike structure in particular, it allows for stability in smaller attractive BECs. Often, this term can be neglected in what is known as the hydrodynamic limit when the interaction energy between particles is larger than the Healing length $\xi = \frac{1}{\sqrt{g\rho}}$. Neglecting $Q$ and putting Eq.(1.19) into a more standard form of the Euler equation by taking a derivative, multiplying by $\rho$ , and collecting all forces into a single pressure term we get:

$$\rho m v\frac{\partial v}{\partial x} = -\frac{\partial V_{\text{ext}}}{\partial x} - g\rho\frac{\partial\rho}{\partial x} - \frac{\partial}{\partial x}\text{Re}(\frac{J_e}{\hbar\Psi}) = -\frac{dP}{dx} \tag{1.20}$$

This form is used in typical acoustic metric derivations, although many include time-dependent terms.

## 1.5 Acoustic Metric

In deriving the acoustic metric, some assumptions are made. We assume the fluid is inviscid, barotropic, and the flow is irrotational. To separate the sound waves from the

condensate flow, we linearise around first-order perturbations in pressure, density and the velocity potential $v = -\nabla\phi$. After manipulations see [33], we end up with the following wave equation:

$$\Box\delta\phi = \frac{1}{\sqrt{-\det(g_{\mu\nu})}}\partial_\mu\left(\sqrt{-\det(g_{\mu\nu})}\, g^{\mu\nu}\partial_\nu\delta\phi\right) = 0 \tag{1.21}$$

Where $g_{\mu\nu}$ is the effective metric and $\Box$ the D'Alembert operator. Rearranging and taking the inverse of the metric gives us the effective metric:

$$g_{\mu\nu} = \frac{\rho}{c_s}\begin{bmatrix} -(c_s^2 - v^2) & -v_j \\ -v_i & \delta_{ij} \end{bmatrix} \tag{1.22}$$

This metric is up to a conformal factor(a length scaling which preserves angles) the same as the Painleve-Gullstrand metric associated with an observer free-falling into a black hole [34]. This means the systems have equivalent null geodesics, which describe the paths taken by massless particles in spacetime. This metric is important for defining the event horizon. It should be noted that the model is only approximate, in the high frequency sector solutions are no longer bound by the horizon. Waves must therefore behave approximately as phonons $\omega \approx ck$ to remain confined.

## 1.6 Examples of Dynamical Instabilities

Dynamical instabilities are best understood through frame-dependent frequency. For example, as a wave approaches a rotating black hole, its frequency appears gravitationally Doppler shifted to a free-falling observer due to spacetime curvature. For certain modes, this shift renders the wave negative-energy near the event horizon, within the ergoregion. To conserve energy, absorption of such modes must be accompanied by emission of an amplified wave. A process known as superradiance. Another example, the Schiff–Snyder–Weinberg (SSW) effect, occurs when bound states dive into the negative-energy continuum and mix with positive-frequency modes, resulting in exponential growth, this is related to the Klein paradox discussed in Sec.(2.2). In either case, the presence of negative energy allows wave amplification, which is a necessary condition for dynamical instability. Secondly, a feedback loop is needed to allow this process to self-amplify. A well-known example is the black hole bomb: placing a reflective mirror around the black hole causes repeated superradiant scattering and exponential amplification of the wave [1]. In our system, finite boundary conditions can support negative-energy bound states, see Sec.(2.5), which may undergo similar amplification due to the boundary conditions.

# 2 Dynamical Instabilities in BdG

In this chapter, we will investigate the features of the quasi-1D finite analogue black holes. We will analyse the dispersive relation, explaining why this allows for negative energy solutions in the laboratory reference frame. We will relate the presence of dynamical instabilities with energetic instabilities, which occur when the energy levels of a system change sign and develop the conditions necessary for DIMs to emerge. Finally, we will present new instabilities found in Neumann/Robin conditions.

## 2.1 Mode Spectrum Analysis

We solve for the eigenfrequencies of Eq.(1.7). For simplicity, we take $g_u = 1$:

$$\omega\sigma_1\Phi = (-\frac{1}{2}\sigma_1\frac{\partial^2}{\partial x^2} - im_u\sigma_3\frac{\partial}{\partial x} + g\sigma_4)\Phi \tag{2.1}$$

In subsonic and supersonic regions, the coupling strength is given by:

$$g = \begin{cases} g_u = 1, & x < 0 \\ g_d = (m_u/m_d)^2, & x > 0 \end{cases} \tag{2.2}$$

The general solution of Eq.(2.1) is a superposition of plane wave $\psi = B_k e^{ikx}$, $\psi^* = C_k e^{ikx}$ or $\Phi = \zeta_k e^{ikx}$. By substituting this plane wave ansatz, we arrive at the familiar Bogoliubov dispersion relation:

$$(\omega')^2 = (\omega - vk)^2 = k^2(\frac{k^2}{4} + g) \tag{2.3}$$

$\omega'$ is the frequency in the co-moving frame and $\omega$ the frequency seen in the rest or laboratory frame. These dispersion relations are shown in Figure (3), where the norm of a mode is determined from the perspective of someone moving with the flow. Meaning, a positive norm should imply positive frequency within this frame. The norm of a mode is conserved as we change reference frame, while the frequency does change when Doppler shifted. This mechanism allows for negative frequencies with positive norm. An important quantity is $\omega_{max}$ defining for a given flow the maximum positive frequency for which there exists a k-wave vector with negative norm and vice versa due to symmetry. This can be found by finding by solving $\frac{\partial\omega}{\partial k} = 0$ in the negative branch, which involves solving a quartic equation and picking the appropriate branch of many solutions.

$$\omega_{max} = \frac{\sqrt{2}\left(2m_u\sqrt{-4g + m_u^2 + m_u\sqrt{8g + m_u^2}} - \sqrt{-8g^2 + 4gm_u^2 + m_u^4 + m_u^3\sqrt{8g + m_u^2}}\right)}{4} \tag{2.4}$$

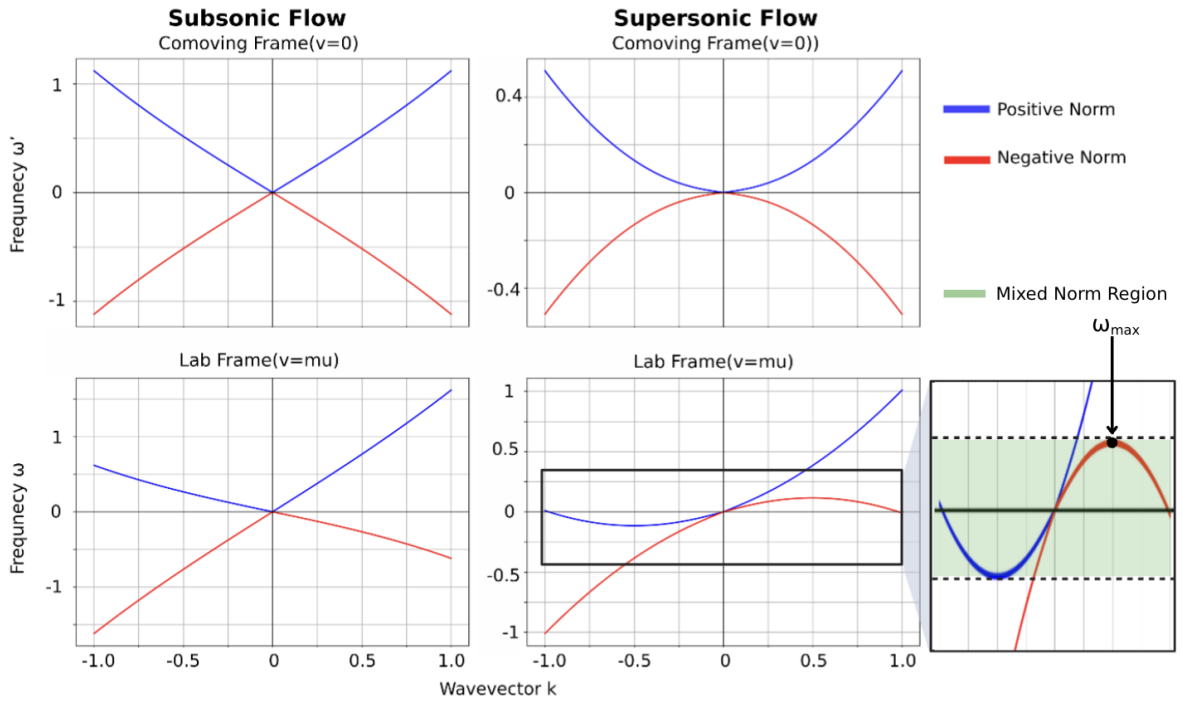


Figure 3: Behaviour of dispersion relation in different velocities and reference frames: The co-moving frames are similar. There are two real roots, where the positive frequency solutions have positive norm and vice versa. In the lab frame, it is different. When the Mach number becomes supersonic, a region exists in which omega has four positive real $k$ roots, two of each norm sign. This figure takes inspiration from [35].

Within $-\omega_{max} < \omega < \omega_{max}$, k has four solutions, two with each norm sign breaking the usual symmetry between frequency and norm. Solving the eigenfrequencies of this problem for any given parameter space is difficult to do analytically, hence we turn to numerical methods. For both regions, there are four possible k solutions, containing both real and imaginary parts. This results in a total of 8 degrees of freedom for a given omega. There are also a total of 8 boundary conditions: two from the boundaries and two from ensuring continuity and derivative continuity at the boundary for both $\psi, \psi^*$. As a given solution can have any multiplicative factor, we can solve these equations numerically to find the allowed eigenfrequencies, and this spectrum will be discrete even if infinite. The general solution for an eigenvector of the system is then:

$$\Phi_\omega(x) = \begin{cases} \sum_{k_u}^{(4)} A_{k_u} \zeta_{k_u} e^{ik_u x}, & x < 0, \\ \sum_{k_d}^{(4)} A_{k_d} \zeta_{k_d} e^{ik_d x}, & x > 0, \end{cases} \tag{2.5}$$

where the constant zeta has the form:

$$\zeta_k = (g/g_u, \omega - m_u k - k^2/2 - g/g_u)^T \tag{2.6}$$

It is not possible, to the writer's knowledge, to solve this equation analytically in terms of an orthogonal basis, so we investigate numerically.

## 2.2 Klein Paradox

In order to understand the following results it is useful to first consider a simplified scattering problem similar to those seen in the Klein-Gordon equation [31]. To do this we restrict ourselves to only some of the 4 total k modes in Eq. (2.7).

$$k = \pm\sqrt{2(m_u^2 - g) \pm 2\sqrt{(g - m_u^2)^2 - \omega^2 + 2m_u\omega\sqrt{1 + \frac{1}{4m_u^2}}}} \tag{2.7}$$

In the subsonic flow, there is a single ingoing mode for which k is real and $\frac{\partial\omega}{\partial k} > 0$. Imposing no specific boundary conditions and instead imposing that this mode scatter into a single reflected and transmitted mode, we can understand the Klein paradox and wave creation.

$$\Phi_\omega(x) = \begin{cases} e^{ik_\omega x} + R_\omega e^{-ik_\omega x}, & x < 0 \\ T_\omega e^{ik'_\omega x}, & x > 0 \end{cases} \tag{2.8}$$

We chose $k'_\omega$ to be the mode which is imaginary when the flow is subsonic, which becomes real when the flow becomes supersonic, as seen from Figure (3), this mode has negative norm. As this is a scattering, we have the following conservation which can be found from the Wronskian:

$$|R_\omega|^2 + |T_\omega|^2 \mathrm{Re}(\frac{k'_\omega}{k_\omega}) = 1 \tag{2.9}$$

Hence, when the flow is entirely subsonic, there is total reflection (noting only in the simplified example), but when $k_\omega$ becomes real, since it has a negative norm, there must be more than total reflection $|R_\omega|^2 > 1$. This is the Klein paradox, which in classical field theory predicts the steady creation of opposite norm waves from a single positive norm incoming wave. In a particle interpretation, this would be the creation of particle-antiparticle pairs. Since in our problem we deal instead with a bound state made of many k-waves, the mathematics is not so simple and cannot be done entirely analytically, but the concept is the same. Waves which are entirely comprised of positive norms can generate waves of mixed norms at the horizon. This scattering concept can be further extended if you consider a wave which is ingoing from the supersonic flow. In this case, a negative norm reflected component can be "trapped" within the supersonic region, since there are no negative norms allowed outside this region. As further negative norm waves are generated by mode conversion, these may constructively or destructively interfere with each other based on the length of the resonant cavity and their phase differences. This is the black hole lasing effect [36]. We shall see that this effect occurs within our

finite system, but that other instabilities also occur with different boundary conditions.

## 2.3 Finite Difference Method & Boundary Conditions

In Figure (4), we summarise the method we use to numerically solve for the eigenfrequencies of the Bogliubov-De-Gennes. Dirichlet boundary conditions are physically the most

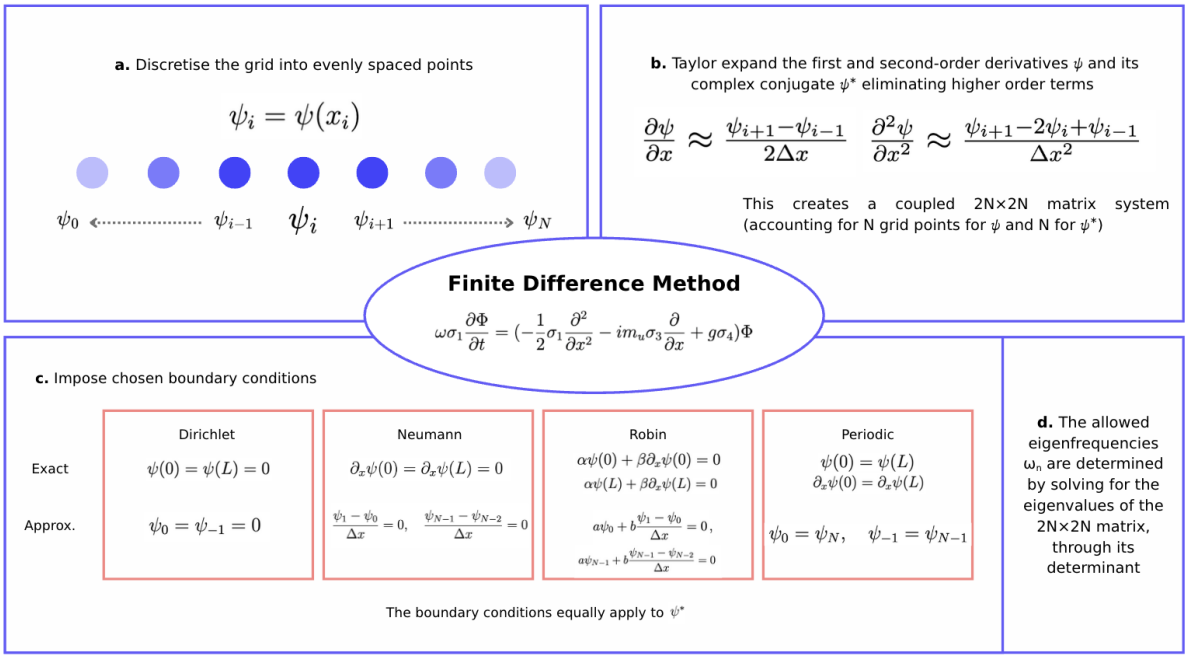


Figure 4: How to model using finite difference. This method is generally second-order accurate, and its validity was confirmed by comparison with other established methods. Since our primary focus is on low eigenfrequencies and long wavelengths, high spatial resolution was not required. $N \approx 200$

natural. These correspond to a confined flow with a supersonic region, which therefore defines an analogue black or white hole. Periodic conditions instead define an infinitely extended flow. If the Mach number is supersonic in either region, then black hole-white hole pairs form in the flow. This setup is similar to that explored in black hole lasers [15]. Neumann boundary conditions, like Dirichlet, are confining, but do not have zero density at the boundary. Robin conditions are a linear combination of Dirichlet and Neumann with each as a limiting case, they can be seen, therefore, as a weaker boundary condition.

## 2.4 Types of DIMs

In the case of $L_1, L_2$ this can be explained by the dispersion relation. As we increase the size of the cavity, the lowest allowed positive eigenfrequency decreases, once this goes below the $\omega_{max}$ the solution space is no longer limited by positive norm solutions. In the presence of negative norm solutions, mode merging can occur. Generally, these solutions

originate from a Galilean transform of the eigenfrequencies in the co-moving frame. An eigenfrequency which decreases with L will first cross the axes at 0 before asymptoting at $-\omega_{max}$ see Fig.(5). Hence, there is for any choice of parameters a minimum length needed

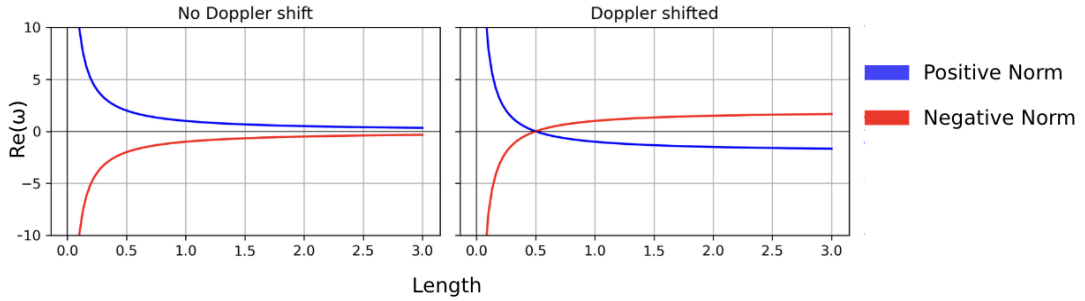


Figure 5: Plots showing how Doppler shift affects eigenfrequencies.

so that the eigenfrequencies of opposite norm cross. Due to the pseudo-Hermitian nature of Eq.(1.8), there are two types of dynamical instabilities. Non-degenerate instabilities occur only at $\omega = 0$, and they come in pairs $(\omega, \omega^*)$. Degenerate instabilities instead appear in quartets $(\omega, \omega^*, -\omega, -\omega^*)$. As we observe that increasing any of the parameters $(L_1, L_2, m_u, m_d)$ leads first to Non-degenerate DIMs see Figure (6).

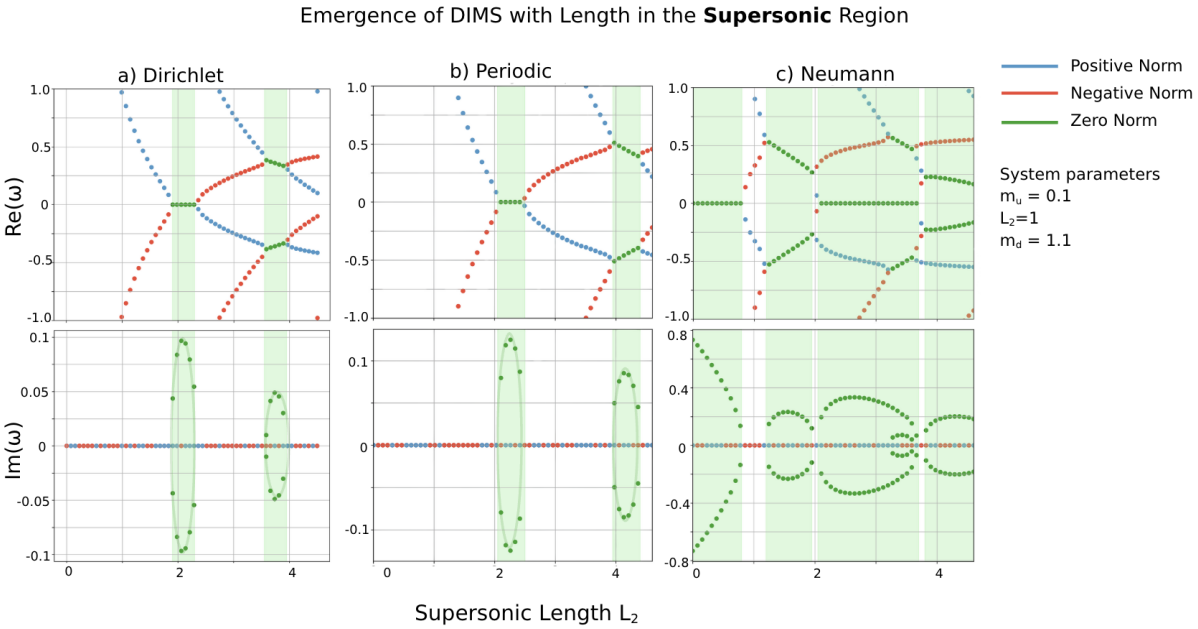


Figure 6: Plot of dynamical instabilities as the length of the supersonic region varies. In this figure, we first observe the emergence of non-degenerate DIMs, followed by the appearance of degenerate DIMs as the cavity length increases. In Neumann boundary conditions, the presence of a supersonic region immediately implies a DIM. Note: the Goldstone mode has been omitted for clarity and was not observed to affect DIMs. The green shaded areas indicate regions of instability.

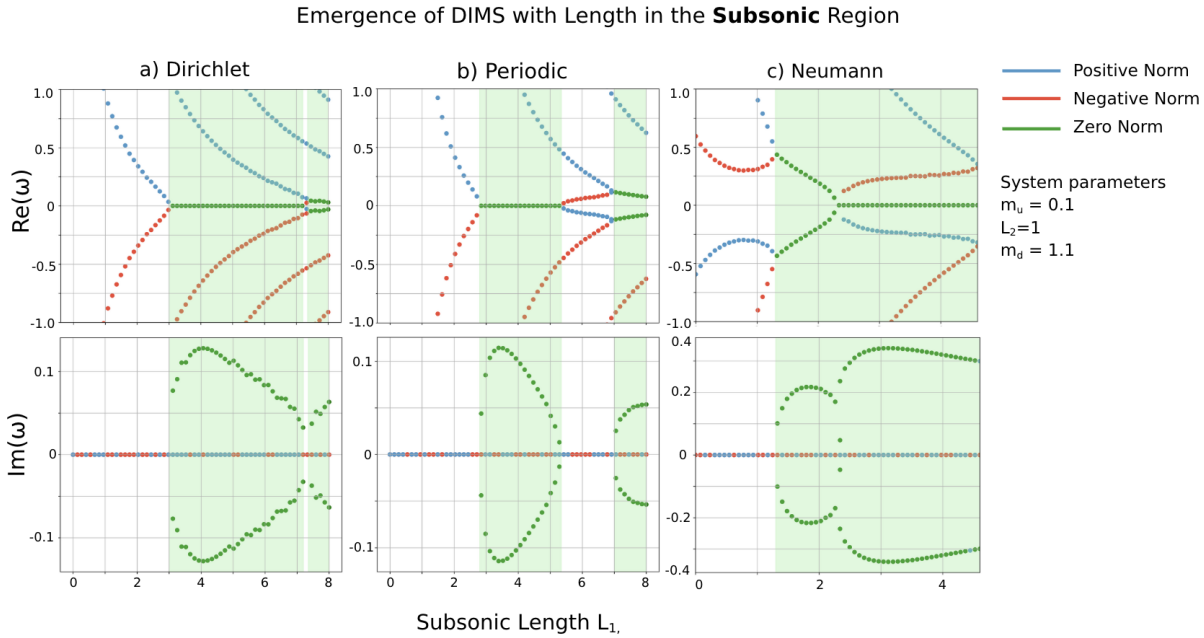


Figure 7: Plot of dynamical instabilities as the length of the subsonic region varies. Compared to a larger supersonic region, we see DIMs occur for larger values of $L_1$ and last for larger spacing, indicating that eigenvalues decrease at a faster rate with increasing supersonic length.

## 2.5 Energetic Instabilities & Landau Velocity

We can transform the $H_{BdG}$ matrix whose eigenvalues give us the allowed eigenfrequencies into $H_E$ which gives us the energy spectrum of our stationary modes [31].

$$H_{BdG} = iJH_E, \quad J = \begin{pmatrix} 0 & 1 \\ -1 & 0 \end{pmatrix} \tag{2.10}$$

$J$ is the symplectic matrix. We note this work is done in classical field theory, so we have not quantised the field, hence any finite amount of this mode can be excited. We have not therefore defined particles. The Bogoliubov-de-Gennes equation contains negative energy solutions, which are usually connected in QFT to the notion of an anti-particle and do not couple to the positive energy spectrum. Energetic instabilities, however, occur when an energy mode changes sign and can couple. For example, Landau instability occurs in a superfluid which crosses the speed of sound, causing excitations within the fluid to become energetically favourable over the ground state of the fluid. These excitations are shown in Figure (8). This, however, is not a sufficient condition, as seen by the fact that purely supersonic flow without a discontinuity or a flow governed by a singular Mach number has exactly the modes satisfying Eq.(2.3). We show the overlap of opposing norms in Figure (9). Interestingly, this seemingly conflicts with the case of Dirichlet and Neumann boundary conditions where dynamical instabilities continuously occur as length

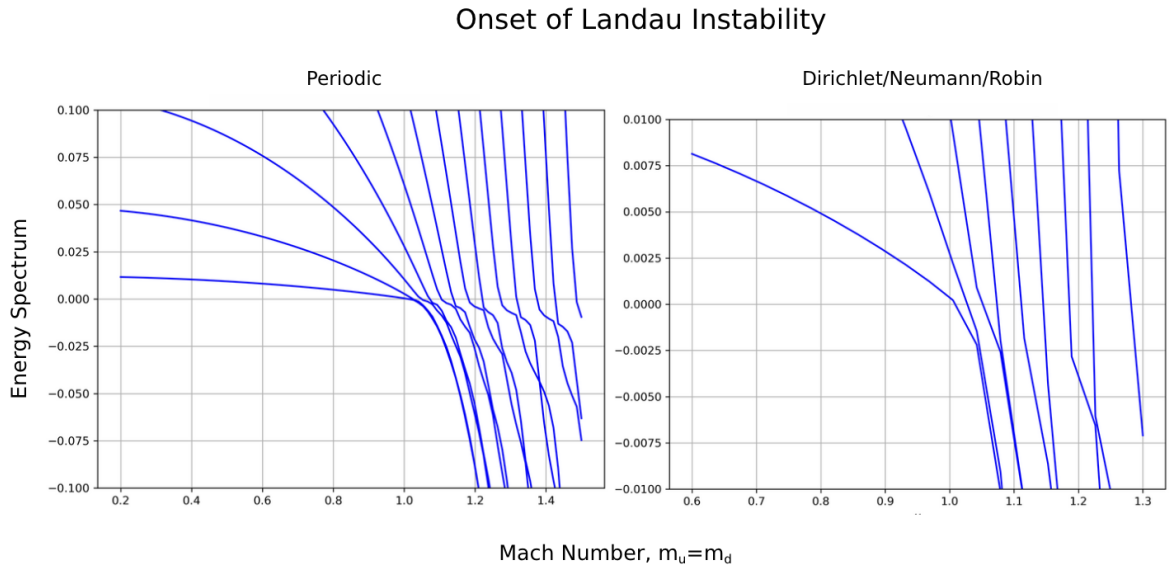


Figure 8: We plot the energy spectrum for a constant Mach number flow. We observe that for periodic boundary conditions, energetic instability occurs as the flow goes supersonic. For all other boundary conditions, the graphs are qualitatively similar. We note that DIMs appear in conjunction with negative energy except for an infinitely extended flow, which is precisely because no mode mixing occurs.

of the supersonic region is increased. However on closer inspection, one notices that the maximum magnitude of the imaginary part of these instabilities decreases with increasing length and one can therefore expect that as $L_2 \to \infty$ the growth rate of the instability vanishes. This illustrates that in the limiting cases, these models are consistent. The presence of a black hole-white hole setup has been shown to produce reflection between the horizons [17].

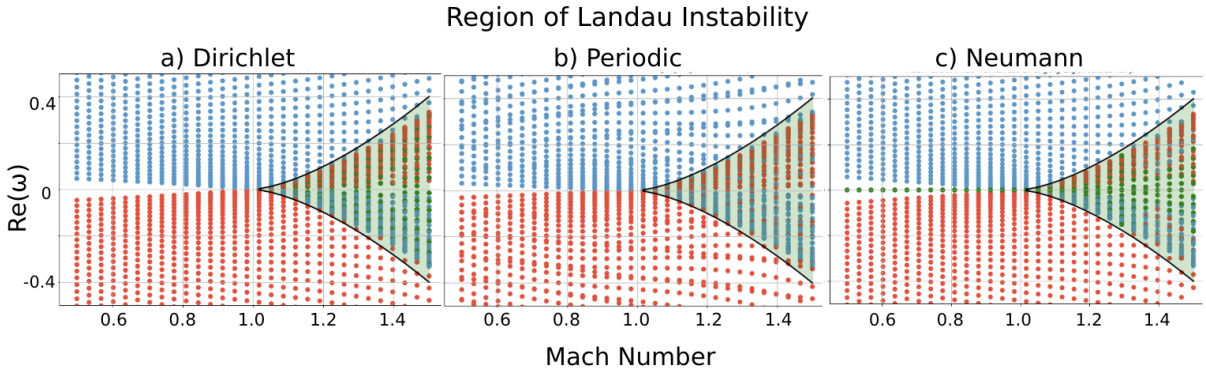


Figure 9: We plot the region of overlap between positive and negative norms in eigenfrequency as the Mach number varies. The Mach number remains constant along the entire flow. Mode mixing occurs only in the green shaded area, $-\omega_{max} < 0 < \omega_{\max}$, since it depends on the up and downstream Mach numbers. We can understand the non-trivial emergence of dynamical instabilities with changing Mach number is due to the shifting of this overlap. We also note the presence of an extra instability in the Neumann case.

We find no difference, qualitatively, between this effect and that found by a confined flow with a single horizon. We therefore conclude that reflection is the secondary condition necessary for the occurrence of DIMs, expanding on the work in [15]. Namely, that we need a mixing of positive and negative norm solutions in the presence of reflective boundaries which send waves back towards the horizon. This allows constructive interference, amplifying these modes exponentially.

## 2.6 Neumann and Robin BCs

In Neumann and Robin BC, an extra instability forms, which crucially does not depend on the presence of an energetic instability, see Figure (10). The origins of this instability are unknown, it arises as we change from Neumann to Dirichlet conditions. We explore by adjusting the coefficients in Robin BC, $\alpha\Phi(L) + \beta\frac{\partial\Phi}{\partial x} = 0$. $\alpha = 0$ corresponds to Neumann conditions and $\beta = 0$[1] corresponds to Dirchlet conditions. BECs analogue model can thus include extra instabilities, not only those arising from lasing. We find no similarities between these differing instabilities and conclude further research is needed.

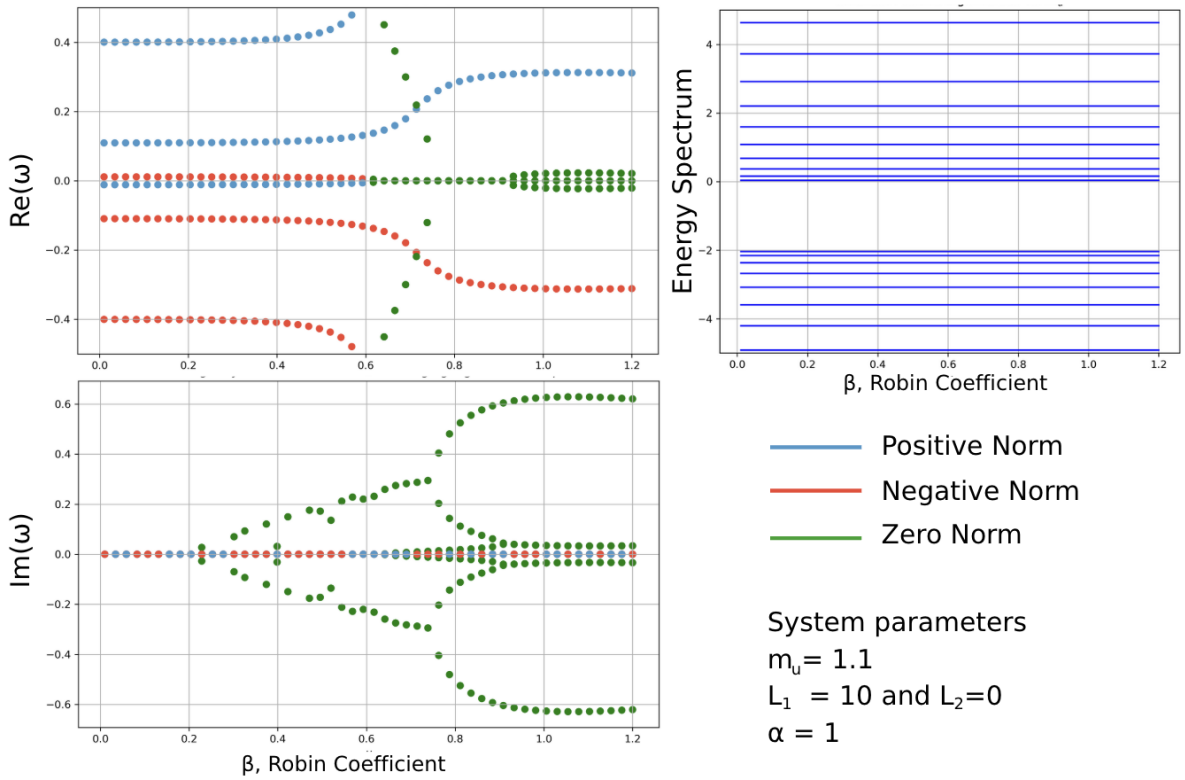


Figure 10: Plots showing dynamical instabilities forming as $\beta$ varies. We see here that the dynamical instabilities take on a very different character from those of the horizon effect. The energy spectrum does not change as the dynamical instabilities occur, and these instabilities split and merge as $\beta$ increases.

[1] In the FDM system $\beta \neq 0$ but instead $\frac{\alpha}{\beta} \to \infty$, we verified this gave the expected result.

# 3 Conclusions and Discussion

## 3.1 Conclusions

This report details our findings on dynamical instabilities in a finite cavity composed of two regions, each with a different Mach number. In this investigation, we identify two types of instabilities: horizon instabilities and boundary condition-dependent instabilities. Horizon instabilities resemble those found in the black hole lasing effect and are close in origin to those important in superradiant effects. We illustrate this with a simplified scattering example for the production of opposite-norm-sign waves. By numerical simulation using Finite Difference Methods(FDM), we observed that for horizon instabilities to occur, a region of supersonic flow is necessary. A supersonic flow allows for negative energy states due to Landau instabilities occurring in BECs. These energetic instabilities, which occur when an energy state changes sign, allow for crossing between positive and negative norm states. If these opposing norm states merge and exponentially grow, then dynamical instability occurs in what we describe as "mode merging".
Additionally, we found it necessary to have a reflective boundary for such an instability to occur. While previous studies report that due to the non-linear dispersion relation Eq.(2.3) mode merging can occur at two horizons, we show that with the presence of a confinement and single horizon or supersonic region, it is possible to create negative norm modes which merge. We report that both mechanisms are largely identical, and we expect that a phase relation can be derived. Such a relation will outline how constructive interference can take place within the system to produce exponential growth, noting that this work has already been done for two-horizon systems [36]. We therefore conclude that these systems should also exhibit similar cases of stimulated Hawking radiation [37, 38]. We clarify the emergence of dynamical instabilities as the Mach number changes, showing that increasing the Mach number in the supersonic region shifts eigenfrequencies, creating a greater overlap between opposing norm modes. In general, as we vary the Mach number, the spacing between eigenfrequencies changes, causing them to couple and decouple.
It was seen that in Neumann and Robin boundary conditions, a new instability occurs, which does not require the presence of a supersonic region. This instability does not occur due to an energetic instability but does appear to affect the presence of other dynamical instabilities, specifically, we find that dynamical instabilities can merge, a phenomenon not seen in purely horizon effects. To the author's knowledge, these instabilities have not been explored in the literature, this finding indicates that the horizon effect is not the only cause of exponential wave amplification. We reinforce that DIMs can occur due to specific boundary conditions imposed on the analogue model, and therefore, if more

complicated experiments are to take place, these effects need to be properly understood.

## 3.2 Discussion

The presence of these instabilities in a large part of the parameter space indicates they cannot be ignored and need to be more rigorously analysed. In solving the linearised Bogoliubov-De-Gennes equation, we ignore non-linear effects. These backreaction effects, which determine change in the physical metric, must be explored to better evaluate the effects these instabilities may have on laboratory measurements. This analysis may lead to these instabilities either invalidating the assumption that the linearised waves are small relative to the background or instead show there exists a natural equilibrium determined by this backreaction, the clarification of this is crucial.

Analogue gravity experiments are likely to be imperative for helping develop our understanding of quantum effects in curved spacetime, and since all experiments are performed in the presence of supersonic flows and a finite boundary, the nature of these instabilities is very important. Additionally, experiments within BECs may be conducted with supersonic Mach numbers or with exotic boundary conditions for many other types of experiments, it is therefore important to understand the phenomena that may present itself within the medium in order for these effects to be taken into account. It may therefore be important to study these models under an even wider range of boundary conditions, such as radiative or Sommerfeld conditions to see if other instabilities arise.

Exceptional points (EPs), at which eigenvalues coalesce and their associated eigenvectors become degenerate, play a central role in understanding the merging of dynamical instabilities observed in our system [39]. The use of bi-orthogonal spectral theory, suitable for Bogoliubov–de Gennes-type equations with indefinite inner products, allows us to analyse these phenomena [28]. By mapping EP2s across the parameter space, including flow velocity, boundary coupling, and cavity length, we may better characterise the transition between stable and unstable regimes. Ultimately, allowing us to build a better picture of EPs in non-Hermitian systems. Finally, if we can perform accurate experiments which match theoretical predictions in analogue systems, we can understand effects we can't observe in real black holes. Informing us further about curved spacetime, which may aid in our search for a theory of quantum gravity.

## 3.3 Acknowledgements

I would like to thank my supervisors, Friedrich Koenig and SangShin Baak, for their support and continued feedback on my research and writing. I would also like to thank Laila Deen for her advice regarding creating figures and presenting work.

# 4 References


[1] W. H. Press and S. A. Teukolsky. "Floating Orbits, Superradiant Scattering and the Black-hole Bomb". In: *Nature* 238.5361 (1972), pp. 211–212. DOI: 10.1038/238211a0.

[2] D. D. Solnyshkov et al. "Quantum analogue of a Kerr black hole and the Penrose effect in a Bose-Einstein condensate". In: *Physical Review B* 99.21 (2019), p. 214511. DOI: 10.1103/PhysRevB.99.214511.

[3] Betül Demirkaya, Tekin Dereli, and Kaan Güven. "Analog black holes and energy extraction by super-radiance from Bose–Einstein condensates (BEC) with constant density". In: *Heliyon* 5.9 (2019), e02497. DOI: 10.1016/j.heliyon.2019.e02497.

[4] Stephen W. Hawking. "Particle Creation by Black Holes". In: *Communications in Mathematical Physics* 43.3 (1975), pp. 199–220. DOI: 10.1007/BF02345020.

[5] W. G. Unruh. "Notes on black-hole evaporation". In: *Physical Review D* 14.4 (1976), pp. 870–892. DOI: 10.1103/PhysRevD.14.870.

[6] S. B Giddings. "Black Holes in the quantum universe". In: *Phil. Trans. R. Soc. A* 377 (2019), p. 20190029. DOI: 10.1098/rsta.2019.0029.

[7] C. Sivaram. "Black hole Hawking radiation may never be observed!" In: *General Relativity and Gravitation* 33.10 (2001), pp. 1751–1753. DOI: https://doi.org/10.1023/A:1002753400430.

[8] Jeff Steinhauer. "Measuring the entanglement of analogue Hawking radiation by the density-density correlation function". In: *Physical Review D* 92.2 (2015), p. 024043. DOI: 10.1103/PhysRevD.92.024043.

[9] W. G. Unruh. "Experimental Black-Hole Evaporation?" In: *Phys. Rev. Lett.* 46 (21 1981), pp. 1351–1353. DOI: 10.1103/PhysRevLett.46.1351.

[10] M. J. Jacquet, S. Weinfurtner, and F. König. "The next generation of analogue gravity experiments". In: *Phil. Trans. R. Soc. A* 378 (2020), p. 20190239. DOI: 10.1098/rsta.2019.0239.

[11] L. J. Garay et al. "Sonic Analog of Gravitational Black Holes in Bose-Einstein Condensates". In: *Physical Review Letters* 85 (2000), pp. 4643–4647. DOI: 10.1103/physrevlett.85.4643.

[12] Jeff Steinhauer. "Observation of quantum Hawking radiation and its entanglement in an analogue black hole". In: *Nature Physics* 12 (2016), pp. 959–965. DOI: 10.1038/nphys3863.

[13] Juan Ramón Muñoz de Nova et al. "Observation of thermal Hawking radiation and its temperature in an analogue black hole". In: *Nature* 569.7758 (2019), pp. 688–691. DOI: 10.1038/s41586-019-1241-0.

[14] C. V. Vishveshwara. "Scattering of Gravitational Radiation by a Schwarzschild Blackhole". In: *Nature* 227 (1970), pp. 936–938. DOI: 10.1038/227936a0.

[15] Florent Michel and Renaud Parentani. "Saturation of black hole lasers in Bose-Einstein condensates". In: *Physical Review D* 88.12 (2013), p. 125012. DOI: 10.1103/PhysRevD.88.125012.

[16] S. Corley and T. Jacobson. "Black Hole Lasers". In: *Physical Review D* 59.12 (1999), p. 124011. DOI: 10.1103/PhysRevD.59.124011.

[17] Ulf Leonhardt and Thomas G. Philbin. "Black Hole Lasers Revisited". In: *arXiv preprint* (2008). arXiv: 0803.0669 [gr-qc]. URL: https://arxiv.org/abs/0803.0669.

[18] Antonin Coutant and Renaud Parentani. "Black hole lasers, a mode analysis". In: *Physical Review D* 81.8 (2010), p. 084042. DOI: 10.1103/PhysRevD.81.084042.

[19] Stefano Finazzi and Renaud Parentani. "Black hole lasers in Bose–Einstein condensates". In: *New Journal of Physics* 12.9 (2010), p. 095015. DOI: 10.1088/1367-2630/12/9/095015.

[20] Ralf Schützhold et al. "Quantum backreaction in dilute Bose-Einstein condensates". In: *Phys. Rev. D* 72 (10 2005), p. 105005. DOI: 10.1103/PhysRevD.72.105005.

[21] Uwe R. Fischer. "Dynamical Aspects of Analogue Gravity: The Backreaction of Quantum Fluctuations in Dilute Bose–Einstein Condensates". In: *Quantum Analogues: From Phase Transitions to Black Holes and Cosmology*. Ed. by W. G. Unruh and R. Schützhold. Vol. 718. Lecture Notes in Physics. Springer, 2007, pp. 93–115. DOI: 10.1007/3-540-70859-6_5.

[22] Sang-Shin Baak, Caio C. Holanda Ribeiro, and Uwe R. Fischer. "Number-conserving solution for dynamical quantum backreaction in a Bose–Einstein condensate". In: *Phys. Rev. A* 106.5 (2022), p. 053319. DOI: 10.1103/PhysRevA.106.053319.

[23] Caio C. Holanda Ribeiro, Sang-Shin Baak, and Uwe R. Fischer. "Existence of steady-state black hole analogs in finite quasi-one-dimensional Bose-Einstein condensates". In: *Physical Review D* 105.12 (2022). DOI: 10.1103/physrevd.105.124066.

[24] Y. Nakamura et al. "Condition for emergence of complex eigenvalues in the Bogoliubov–de Gennes equations". In: *Physical Review A* 77.4 (2008). ISSN: 1094-1622. DOI: 10.1103/physreva.77.043601.

[25] Jean Macher and Renaud Parentani. "Black-hole radiation in Bose-Einstein condensates". In: *Physical Review A* 80.4 (2009). DOI: 10.1103/physreva.80.043601.

[26] Erwin Madelung. "Quantentheorie in hydrodynamischer Form". In: *Zeitschrift für Physik* 40 (1927), pp. 322–326. DOI: 10.1007/BF01400372.

[27] Ali Mostafazadeh. "Pseudo-Unitary Operators and Pseudo-Unitary Quantum Dynamics". In: *Journal of Mathematical Physics* 45.3 (2004), pp. 932–946. DOI: 10.1063/1.1646448.

[28] Q. Z. Lv et al. "Bosonic pair creation and the Schiff-Snyder-Weinberg effect". In: *Physical Review A* 93.1 (2016), p. 012119. DOI: 10.1103/PhysRevA.93.012119.

[29] János Bognár. *Indefinite Inner Product Spaces*. Vol. 78. Ergebnisse der Mathematik und ihrer Grenzgebiete. 2. Folge. Berlin, Heidelberg: Springer-Verlag, 1974. DOI: 10.1007/978-3-642-65567-8.

[30] Kurt Gottfried and Tung-Mow Yan. *Quantum Mechanics: Fundamentals*. 2nd. Berlin: Springer, 2003. ISBN: 9780387220239.

[31] Antonin Coutant, Florent Michel, and Renaud Parentani. "Dynamical instabilities and quasi-normal modes, a spectral analysis with applications to black-hole physics". In: *Classical and Quantum Gravity* 33.12 (2016), p. 125032. DOI: 10.1088/0264-9381/33/12/125032.

[32] Carlos Barceló, S Liberati, and Matt Visser. "Analogue gravity from Bose-Einstein condensates". In: *Classical and Quantum Gravity* 18.6 (2001), pp. 1137–1156. DOI: 10.1088/0264-9381/18/6/312.

[33] C Barcelo, S Liberati, and M Visser. "Analogue Gravity". In: *Living Revs. Relativity* 8.12 (2005). http://www.livingreviews.org/lrr-2005-12 : cited 07/01/2025. DOI: 10.12942/lrr-2005-12.

[34] Andrew J.S. Hamilton and Jason P. Lisle. "The River Model of Black Holes". In: *American Journal of Physics* 76.6 (2008), pp. 519–532. DOI: 10.1119/1.2830526.

[35] Raul Aguero-Santacruz and David Bermudez. "Negative frequencies and negative norms in analogue Hawking radiation systems". In: *Comptes Rendus. Physique* 25.S2 (2024), pp. 1–17. DOI: 10.5802/crphys.177.

[36] Thomas G. Philbin et al. "Fiber-Optical Analog of the Event Horizon". In: *Science* 319.5868 (2008), pp. 1367–1370. DOI: 10.1126/science.1153625.

[37] Jeff Steinhauer. "Observation of self-amplifying Hawking radiation in an analog black hole laser". In: *Nature Physics* 10.11 (2014), pp. 864–869. DOI: 10.1038/nphys3104.

[38] Jeff Steinhauer and Juan Ramón Muñoz de Nova. "Self-amplifying Hawking radiation and its background: A numerical study". In: *Physical Review A* 95.3 (2017), p. 033604. DOI: 10.1103/PhysRevA.95.033604.

[39] W. D. Heiss. "Exceptional points of non-Hermitian operators". In: *Journal of Physics A: Mathematical and General* 37.6 (2004), pp. 2455–2464. DOI: 10.1088/0305-4470/37/6/034.